Macromolecules
ARTICLE

*Macromolecules* **2009**, *42*, 9103–9110 **9103**
DOI: 10.1021/ma901707s

# Control of Coalescence in Clusters of Elastomer Colloids through Manipulation of Polymer Composition

**Cornelius Gauer, Hua Wu, and Massimo Morbidelli***

*Institute for Chemical and Bioengineering, Department of Chemistry and Applied Biosciences, ETH Zurich, 8093 Zurich, Switzerland*

*Received July 31, 2009; Revised Manuscript Received October 9, 2009*

ABSTRACT: The effect of rigid polymer content, tetrafluoroethylene (TFE), within elastomer polymer on the coalescence behavior of suspended rubbery particles during fast, diffusion-limited cluster−cluster aggregation (DLCA) has been studied in this work. This is achieved by first measuring in situ the time evolution of the average hydrodynamic radius of the clusters using dynamic light scattering and then applying the Smoluchowski kinetic approach, based on population balance equations (PBE), to simulate the measured kinetics using the only unknown parameter, the fractal dimension (representing the structure of the clusters), as the fit parameter. It is found that the so-obtained fractal dimension is well correlated to the TFE fraction of the polymer, with a value equal to 3 in the absence of TFE and 1.7 when 75% TFE is present in the polymer. The former indicates full coalescence of particles during aggregation and the latter negligible coalescence, corresponding to typical fractal clusters obtained under DLCA conditions. When the aggregation temperature is varied from 25 to 70 °C, no changes in the predicted values of the fractal dimension have been observed. This is explained by considering that TFE is present in the form of rigid TFE-rich domains, dispersed in the flexible elastomer phase within the particles, whose content determines the coalescence extent during aggregation. The cluster structure information obtained from the PBE simulations is then confirmed by cryogenic electron microscopy. It is therefore concluded that measuring the DLCA kinetics combined with the PBE simulations can be well applied to investigate the coalescence behavior of elastomer particles.

## 1. Introduction

Elastomer colloids are synthetic nanometer-sized soft particles in dispersion, which may undergo deformation or even coalescence, when they have physical contact. Such behavior can be advantageous, e.g., in latex film formation,[1−3] or disadvantageous since it may lead to uncontrolled cluster growth during solid−liquid separation for recovery of the elastomer after polymerization. Above the glass transition temperature, $T_g$, elastomer may flow (polymer chain interdiffusion) much before reaching its liquid state.[1,4,5] In recent studies,[6,7] it has been found that fluorinated elastomer particles with $T_g \approx -20$ °C coalesce during their aggregation at 25 °C. In practical applications, elastomers are often manipulated through the composition of the polymerized monomers to tune the material properties, e.g., polymer viscosity, glass transition, etc., which alters the polymer flowability and thus particle coalescence. It is therefore of practical importance to know the effect of polymer composition on the coalescence disposition of elastomer particles.

Fast, diffusion-limited cluster−cluster aggregation (DLCA) under stagnant conditions is a rather simple and well-studied physical process.[8−10] It can be realized by completely destabilizing the colloidal system using a salt. Under DLCA, the only transport mechanism for particle collision is diffusion, and the sticking probability is close to unity for all particles. Numerous studies[10−26] have shown that for rigid particles this process follows a certain universal behavior (e.g., power-law time evolution of average cluster size, and the cluster fractal dimension $D_f$ varies about 1.7 to 1.8). Moreover, it has been proven[14,16,17,22−25,27,28] that the Smoluchowski kinetic approach, based on population balance equations (PBE), can well reproduce the time evolution of the average cluster size, with the $D_f$ value independently measured as the only model parameter. The same approach has been recently used to model a DLCA process of elastomer particles.[7] It was found that also in the case of full coalescence the time evolution of the average hydrodynamic radius of the clusters, determined in situ by dynamic light scattering (DLS), is correctly predicted if $D_f = 3$ is used. All these results motivate us to consider that by measuring the DLCA kinetics combined with the PBE simulations, using the fractal dimension as the only fit parameter, one can well quantify the coalescence extent of elastomer particles based on the predicted $D_f$ value.

Therefore, in this work we apply this methodology to investigate the coalescence behavior of five fluorinated elastomer colloids of different polymer composition. For independent verification, the cluster structure is also spot-checked by image analysis of electron micrographs prepared in cryogenic conditions. The obtained results confirm the reliability of the proposed methodology.

## 2. Theoretical Background

**2.1. The PBE Model.** Aggregation, resulting from irreversible sticking of colliding particles, can be conveniently described as subsequent second-order processes by following the Smoluchowski approach.[29] The mass or population balance equations (PBE) may be written in discrete form as[29−32]

$$\frac{dN_i}{dt} = -\sum_{j=1}^{j_{max}} K_{i,j} N_i N_j + \frac{1}{2}\sum_{j=1}^{i-1} K_{i-j,j} N_{i-j} N_j \qquad (1)$$

where $N_i$ is the number concentration of $i$-fold clusters, i.e., composed of $i$ primary particles, and $K_{i,j}$ is the kernel (matrix of

*To whom correspondence should be addressed: e-mail morbidelli@chem.ethz.ch; Tel 0041-44-6323034.



Published on Web 10/29/2009

rate constants). For aggregation of completely destabilized particles, where the sticking probability is close to unity and independent of the cluster size, the typical form of the kernel is[30,31,33−37]

$$K_{i,j} = \frac{K_B}{W}\frac{(i^{1/D_f} + j^{1/D_f})(i^{-1/D_f} + j^{-1/D_f})}{4} \quad (2)$$

In the first term, $K_B$ is the so-called Smoluchowski rate constant for primary particles[29,35]

$$K_B = \frac{8kT}{3\mu_l} \quad (3)$$

where $kT$ is the thermal energy and $\mu_l$ the dynamic viscosity of the dispersant. $W$ in eq 2 is the Fuchs stability ratio, which accounts for remaining colloidal interactions,[35,38−43] including the hydrodynamic resistance caused by the squeezing of the fluid during particle approach. Under DLCA conditions, since electrostatic repulsion is completely screened, $W$ is basically a constant, with a typical value around 2.[3,16,33,34,44−49] The second term in eq 2 represents the effect of the sizes of colliding clusters on the aggregation rate through their diffusivity and colliding cross-section area, which is obviously a function of the cluster structure expressed by the fractal dimension, $D_f$. It follows from eq 2 that aggregation of small with large clusters is preferred, leading to a rather narrow (bell shaped), self-preserving cluster mass distribution (CMD).[31,34,50−52]

The most attractive feature of the kinetic approach can be seen when we rewrite the PBE (eq 1) in dimensionless form:[34,53]

$$\frac{dX_i}{d\tau} = -\sum_{j=1}^{j_{max}} \beta_{i,j} X_i X_j + \frac{1}{2}\sum_{j=1}^{i-1} \beta_{i-j,j} X_{i-j} X_j \quad (4)$$

where $X_i$ ($= N_i/N_{1,0}$) is the dimensionless cluster number concentration and

$$\tau = tN_{1,0}K_B/W \quad (5)$$

defines the dimensionless time, with $N_{1,0}$ ($= 3\phi/[4\pi R_p^3]$) the initial number concentration of primary particles. Then, the kernel (eq 2) is reduced to

$$\beta_{i,j} = \frac{(i^{1/D_f} + j^{1/D_f})(i^{-1/D_f} + j^{-1/D_f})}{4} \quad (6)$$

It can be seen from eqs 4−6 that with the dimensionless time the evolution of the dimensionless CMD depends only on one parameter, $D_f$. This implies that if DLCA processes produce clusters of the same structure ($D_f$), no matter which material, concentration and size of the particles, and coagulant type one is using, all the kinetic data (e.g., time evolution of the average hydrodynamic radius) collapse onto a single master-curve, when they are plotted in terms of the dimensionless time $\tau$.[7,18,24,53−55] It is this feature that motivates us to use DLCA experiments for investigating the coalescence behavior of elastomer particles.

**2.2. Simulation.** The quantity that we choose to monitor the DLCA kinetics is the time evolution of the average hydrodynamic radius of the growing clusters, $\langle R_h \rangle$, which is measured by in situ dynamic light scattering at a given angle, $\theta$, or scattering wavevector, $q$. Then, the connection between the CMD, $N_i$ or $X_i$, computed from the PBE, and $\langle R_h \rangle$ is given by[56]

$$\langle R_h \rangle = \frac{\sum N_i i^2 P_i(q)}{\sum N_i i^2 P_i(q) R_{h,i}^{-1}} \quad (7)$$

where $P_i(q)$ and $R_{h,i}$ are the form factor and hydrodynamic radius of the cluster with mass $i$. For a spherical cluster, $P_i(q)$ is calculated according to Lorenz−Mie theory[57,58] and $R_{h,i} = i^{1/3}R_p$ ($R_p$ is the radius of the primary particles). In the case of a fractal cluster, $P_i(q) = P_1(q)S_i(q)$, where $P_1(q)$ is the form factor of the primary particles and $S_i(q)$ the cluster structure factor, computed via the Fisher−Burford expression in this work[59,60]

$$S_i(q) = \left(1 + \frac{2q^2 R_{g,i}^2}{3D_f}\right)^{-D_f/2} \quad (8)$$

where $R_{g,i}$ is the cluster radius of gyration. Both $R_{h,i}$ and $R_{g,i}$ of the individual clusters are calculated based on $D_f$ as given in the literature.[61,62]

The computation of the CMD from eqs 1−3 is accomplished on a grid structure, linear for the first 10 integer sizes and then logarithmic.[32] Convergence of the numerical solution and self-preserving behavior of the calculated CMD have been verified previously.[63] Simulation of the $\langle R_h \rangle$ evolution is achieved by setting a proper value for the fractal dimension $D_f$.

## 3. Experiments

**3.1. Colloid Aggregation.** *The Stable Colloids.* All the latices used are aqueous dispersions of fluorinated elastomer particles, supplied by Solvay Solexis (Italy), which are produced by copolymerization of vinylidene fluoride and hexafluoropropylene with different amounts of tetrafluoroethylene (TFE). Even though the TFE contents range from 0 to about 75%, the polymer phases have a similar glass transition temperature, $T_g$, of approximately −20 °C, unless specified differently. On the basis of the supplier information, viscosity differences are characterized by the so-called Mooney viscosity $\mu_M$ in terms of ML(1 + 10) at 121 °C, measured according to the standard test method ASTM D1646.

The first two colloids are made of TFE free particles, referred to as TFE0-A and TFE0-B, respectively, synthesized via emulsion polymerization and stabilized with perfluoropolyether-based carboxylic surfactants. Both colloids consist of rather monodisperse primary particles with radii of $R_p$ = 60 and 55 nm (as measured by light scattering) for TFE0-A and TFE0-B latices, respectively. Because of differences in polymer molecular weight, the corresponding Mooney viscosities of the two particle types are different, $\mu_M$ = 27 and 101 MU, respectively.

The third latex is similar to the above two but contains 20% TFE in the polymer phase and is accordingly denoted as TFE20. It is stabilized by the same surfactants, but also a small amount of fixed charges (20% of the total charges) exists due to dissociation of polymer chain end groups. Those particles have a $\mu_M$ value of 66 MU and a radius of $R_p$ = 31 nm.

The last two latices contain a TFE fraction of about 75% in the polymer phase; thus, they are termed as TFE75-A and TFE75-B. Both are produced by surfactant-free polymerization, thus stabilized only by the fixed charges originating from the dissociation of carboxylic end groups of the polymer chains. The TFE75-A has a Mooney viscosity of $\mu_M$ = 78 MU and $T_g \approx$ 0 °C, while TFE75-B has $\mu_M$ = 200 MU and $T_g \approx -20$ °C. The primary particles of both latices are rather monodisperse and have a similar size with $R_p \approx$ 100 nm.

*Aggregation Experiments.* The colloids were completely destabilized by protonation of the carboxylic groups on the surface

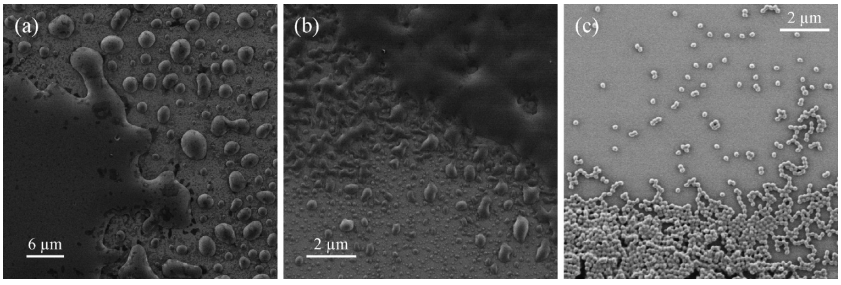


**Figure 1.** Conventional SEM images, obtained by drying of stable (a) TFE0, (b) TFE20, and (c) TFE75 latices at 25 °C. Film formation, due to particle fusion, indicates sufficient polymer flowability for the first two latices. In the third case (TFE75 latex) the primary particles resist against capillary pressure upon drying and conserve their identity, which indicates much higher polymer rigidity.

using nitric acid ($HNO_3$) at sufficiently high concentrations (1−5 times of the critical coagulant concentration, CCC) to surely establish aggregation under the DLCA regime. The original latices as well as the $HNO_3$ solution (analytical grade) were diluted properly with deionized water, purified through a Millipore Simpak 2 column, and filtered through 0.1 $\mu$m Acrodisc syringe filters (Pall, UK), before pouring them together at a ratio of 1 to 4. The final particle volume fractions were $\phi = 3.0 \times 10^{-5}$ and $1.0 \times 10^{-5}$ for TFE0-A and TFE0-B, $\phi = 5.0 \times 10^{-5}$ for the TFE20, and $\phi = 5.0 \times 10^{-6}$ and $1.0 \times 10^{-5}$ for TFE75-A and TFE75-B, respectively. After mixing the colloid with the coagulant solution, the aggregation system (50 mL) was equilibrated for a few seconds before it was portioned into two glass vials. One vial was used for particle size measurement by dynamic light scattering, and the second was stored upside-down. The vials were turned and exchanged for measurement every 10−20 min. Such a procedure is necessary in order to prevent effects of particle sedimentation, which is possible due to the rather high polymer densities (about 2 kg/L) with respect to water. For experiments at temperatures above 25 °C, all solutions and dispersions were stored in a temperature-controlled chamber, and also the light scattering cell was heated through an external circuit with a thermostat.

It should be noted that since the refractive index of the TFE75 particles (near 1.34) is very close to that of water, the intensity of the light scattered by the colloids is too low to get reasonable statistics for the light scattering measurements. Thus, we have added urea into the system (at a level of 2.0 mol/L) to increase the difference in refractive index between the particles and the dispersant. Such a modification is unnecessary in the cases of TFE0 and TFE20 particles, which have a refractive index of about 1.37.

**3.2. Colloid Characterization.** *Dynamic Light Scattering.* The average cluster size of the aggregating dispersions was monitored in situ by dynamic light scattering (DLS).[56,64,65] The employed solid-state laser, Ventus LP532 (Laser Quantum, UK), emits a beam of $\lambda_0 = 532$ nm wavelength, and the scattered light was detected at an angle of $\theta = 90°$ in a BI-200SM goniometer (Brookhaven Instruments). The corresponding scattering vector is defined by $q = 4\pi n_0/\lambda_0 \sin(\theta/2)$, with $n_0$ representing the refractive index of the dispersant. The measured intensity trace autocorrelation function was processed by the BI-9000AT digital correlator and software (Brookhaven Instruments) to return the average translational diffusivity, $\langle D \rangle$, which gives the average hydrodynamic radius of the clusters according to the Stokes−Einstein relation:

$$\langle R_h \rangle = \frac{kT}{6\pi\mu_1\langle D \rangle} \tag{9}$$

Viscosity and refractive index of the disperse media for all the aggregating systems, modified by coagulant and urea, were estimated based on information in the literature.[66]

*Electron Microscopy and Image Analysis.* Soft polymer particles tend to deform and coalesce when they get into contact, e.g., by capillary forces when the latex is dried.[1,2] As can be seen from the conventional scanning electron microscopy (SEM) images, presented in Figure 1, upon drying at ambient conditions (25 °C), the TFE0 and the TFE20 particles spread and form continuous polymer films, while the TFE75 particles do not. However, at least some deformation can be observed for the TFE75 particles. Therefore, to correctly evaluate the structure of the elastomer aggregates during aggregation, we have vitrified and visualized the samples in supercooled conditions (cryo-SEM).[67]

For sample preparation, a droplet of an aggregating dispersion is fixed by a 10 $\mu$m gold grid (spacer) between two sapphire discs and then frozen in a high-pressure freezing machine, HPM 010 (BAL-TEC, Liechtenstein), at about −160 °C. The vitrified specimen is transferred via the BAL-TEC airlock shuttle system VCT 100[68] to the freeze-etching unit BAF 060 from BAL-TEC, where the continuous phase is sublimated under high vacuum at −80 °C (within half an hour) followed by coating with tungsten (≤3 nm). Images are recorded on a Gemini 1530 FEG scanning electron microscope (Zeiss, Germany) equipped with a cold stage.

Because of the very elaborate preparation work, the described procedure has been applied only to spot-check dispersions containing large aggregates (i.e., > 1 $\mu$m) at 25 °C. The obtained micrographs allow an independent determination of the cluster structure by analysis of the projected areas. Note that dense and tenuous aggregates require different ways of extracting the three-dimensional fractal dimension, $D_f$. For dense objects with $D_f > 2$, one may measure the projected perimeter, $P$, and the area, $A$, of several clusters and scale them according to[69,70]

$$A \propto P^{2/D_{pf}} \tag{10}$$

where $D_{pf}$ denotes the perimeter based two-dimensional fractal dimension, which can be converted into the desired $D_f$, through semiempirical correlations given in the literature.[70,71] In the case of tenuous aggregates, one can exploit the fact that for $D_f < 2$ the projection area is proportional to the cluster mass, $M$.[9,72] Then, evaluation of the area or mass for characteristic sizes, $L$, (box count method[8,72−74]) allows to extract $D_f$ from the scaling[8,9,69,74]

$$M \propto L^{D_f} \tag{11}$$

The free software, ImageJ (http://rsbweb.nih.gov/ij/), has been applied to convert cryo-SEM into binary images and to measure the perimeter and the area. Moreover, the software provides a tool to extract the fractal dimension,[75] which has been used after calibration of its operating parameters.

## 4. Results and Discussion

**4.1. DLCA Kinetics of the TFE-Free Elastomer Colloids.** Aggregation experiments with the two TFE0-latices were carried out at 25 °C at different $HNO_3$ concentrations to first

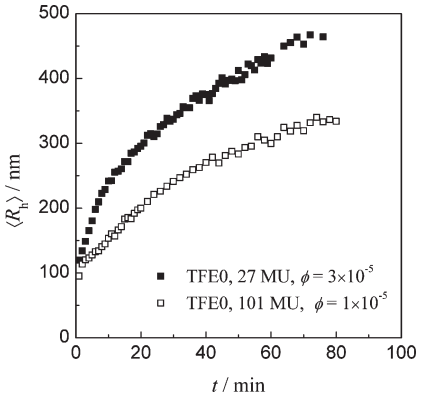


**Figure 2.** Time evolutions of the average hydrodynamic radius, $\langle R_h \rangle$, for TFE0-A latex (■) at $\phi = 3.0 \times 10^{-5}$ and TFE0-B latex (□) at $\phi = 1.0 \times 10^{-5}$, under DLCA conditions at $T = 25$ °C, destabilized by $HNO_3$.

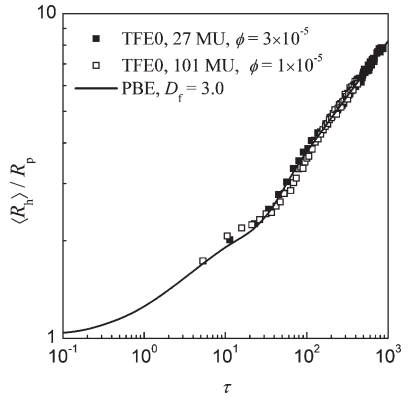


**Figure 3.** $\langle R_h \rangle$ evolutions in Figure 2, replotted as a function of the dimensionless time $\tau$, defined by eq 5. The solid curve is the PBE simulation with $D_f = 3.0$.

determine the critical coagulant concentration, CCC, above which the size evolutions become independent of the $HNO_3$ concentration, and thus to establish the DLCA regime. Both TFE0-A and -B latices have the same CCC of about 0.3 mol/L $HNO_3$, as is expected because similar amounts of the carboxylic surfactant have been used. Then, time evolutions of the average hydrodynamic radii, $\langle R_h \rangle$, have been determined for at least three $HNO_3$ concentrations above the CCC (in the range of 0.3−1.5 mol/L). The results were then averaged and are shown in Figure 2. The obvious faster size evolution of the TFE0-A with respect to the TFE0-B latex results from its particle volume fraction that is 3 times larger. As discussed in the Theoretical Background section, a proper comparison in the aggregation kinetics between the two latices is obtained by plotting the $\langle R_h \rangle$ values as a function of the dimensionless time $\tau$ defined by eq 5, which includes all the effects of variations in particle concentration, temperature, viscosity, etc., on the aggregation rate. Note that we use $W$ values close to 2 in order to get the best overlapping of the kinetic data in $\tau$. The possible small tuning in the $W$ value reflects all kinds of errors during the course of the experiments.

The result of replotting the kinetic data in Figure 2 as a function of $\tau$ is shown in Figure 3 (symbols). It turns out that the two sets of $\langle R_h \rangle$ data from the TFE0-A and -B latices collapse onto a single master-curve. This indicates that the DLCA of the TFE0-A and -B latices follows the same kinetics, and more precisely, the clusters formed by the two latices have the same structure ($D_f$). The next step is to estimate the $D_f$ value through simulation of the master-curve using the PBE

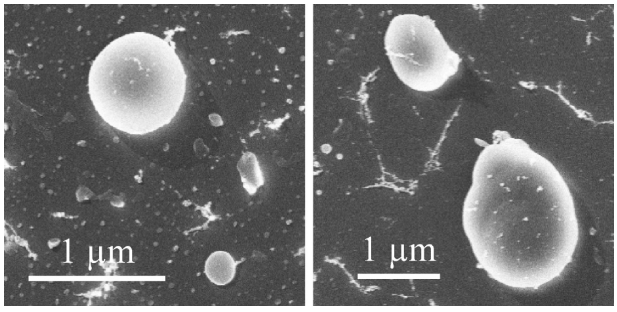


**Figure 4.** Cryo-SEM images of the clusters formed by the TFE0-A latex particles in DLCA at 25 °C.

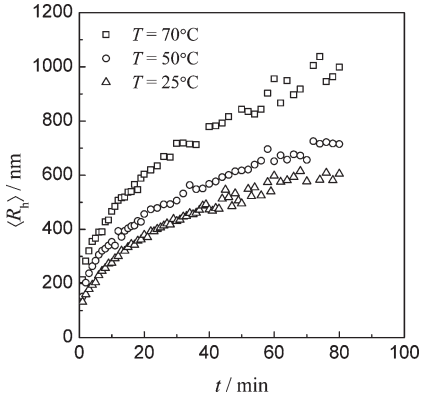


**Figure 5.** Time evolutions of $\langle R_h \rangle$ for DLCA of the TFE20 latex at $\phi = 5.0 \times 10^{-5}$, destabilized by $HNO_3$ at three different temperatures.

approach, where $D_f$ is the only fit parameter. The excellent agreement of the calculated result is shown in Figure 3 by the solid curve, and the obtained value for the fractal dimension is $D_f = 3.0$. Moreover, it is well-known[10,12,14−18,20,22−26,72] that in DLCA the size evolution follows the power law, and the scaling exponent is given by $1/D_f$. In fact, the log−log plot of our data in Figure 3 in the region of large $\tau$ values has a slope of 1/3.

From the obtained $D_f$ value of 3, we can conclude that complete coalescence occurs during the DLCA process for the TFE-free elastomer particles in TFE0-A and -B latices at 25 °C, regardless of different polymer viscosities ($\mu_M = 27$ and 101 MU, respectively).

To prove the cluster structure information from the PBE simulations, cryo-SEM images of clusters formed after an aggregation time of 60 min in the case of the TFE0-A latex are presented in Figure 4. It is clear from the sphere-like shape of the clusters that the elastomer particles coalesce completely upon aggregation at 25 °C; thus $D_f = 3.0$ is confirmed.

**4.2. DLCA Kinetics of the Low TFE Elastomer Colloid.** The colloidal system TFE20, with 20% TFE in the polymer phase was also destabilized by $HNO_3$. Similar to the TFE0-A and -B latices, the CCC for $HNO_3$ is again about 0.3 mol/L. The DLCA experiments were conducted at a $HNO_3$ concentration of 1.0 mol/L and at three temperatures of 25, 50, and 70 °C. Figure 5 displays the $\langle R_h \rangle$ evolutions, obtained by averaging at least two runs. The results clearly indicate that the aggregation rate increases as temperature increases. To examine whether the faster aggregation rate due to higher temperature results only from decreasing dispersant viscosity or also from a cluster structure variation with temperature, let us again plot the $\langle R_h \rangle$ evolutions in Figure 5 as a function of the dimensionless time $\tau$, as shown in Figure 6. Note that in $\tau$ the viscosity values for the disperse medium

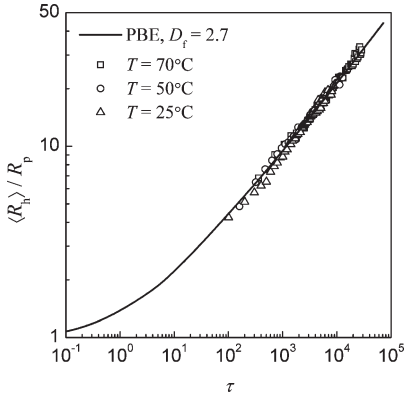


**Figure 6.** All the $\langle R_h \rangle$ data in Figure 5 replotted as a function of $\tau$, where the solid curve is the PBE simulation with $D_f = 2.7$.

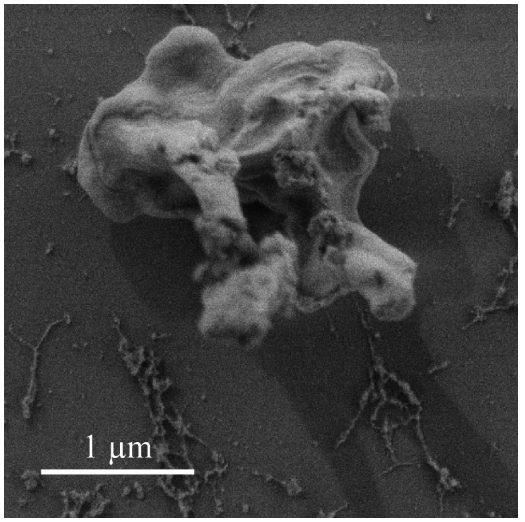


**Figure 7.** Cryo-SEM image of a typical cluster formed by the TFE20 latex particles in DLCA at 25 °C.

were estimated based on the $HNO_3$ aqueous solution,[66] which are $\mu_l = 0.91$, 0.56, and 0.41 mPa s at 25, 50, and 70 °C, respectively. It is remarkable to see that all the $\langle R_h \rangle$ data obtained at three different temperatures collapse onto a single master-curve, revealing that the differences in Figure 5 are indeed only due to temperature and dispersant viscosity effects, and the clusters formed at the three temperatures have the same structure.

Again the $\langle R_h \rangle$ evolution in the double-logarithmic plane in Figure 6 follows the power law at large $\tau$ values, and considering that its slope equals $1/D_f$, we obtain a $D_f$ value of 2.7. In fact, by applying the PBE approach to simulate the $\langle R_h \rangle$ evolution in Figure 6, as shown by the solid curve, we do obtain the same fractal dimension, $D_f = 2.7$. Since the obtained $D_f$ value is smaller than 3 but substantially larger than 1.7, as would be typical for clusters of rigid particles formed under DLCA conditions, we can conclude that considerable coalescence does occur for the TFE20 particles, but its extent is smaller than that in the case of TFE0 particles. This can be attributed to the presence of 20% TFE.

The cryo-SEM technique has also been used to independently validate the structure of TFE20 clusters. The image, shown in Figure 7, indicates strong coalescence of the TFE20 particles, but obviously the cluster is not spherical, confirming incomplete coalescence. By evaluating the projection area and perimeter of 40 objects, we have obtained the scaling of area versus perimeter, as presented in Figure 8.

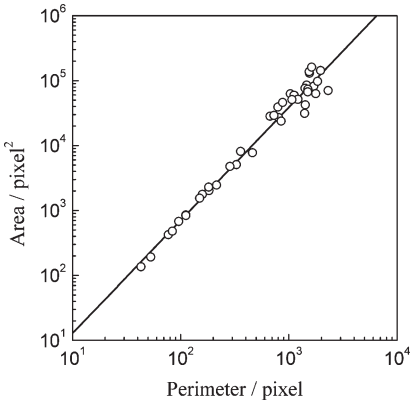


**Figure 8.** Power-law scaling between perimeter and projection area obtained from image analysis of 40 clusters formed by the TFE20 latex, as shown in Figure 7, which allows to estimate the two-dimensional perimeter-based fractal dimension $D_{pf}$.

The corresponding slope of the double-logarithmic plot is equal to $2/D_{pf}$ (= 1.71 in Figure 8), which defines the two-dimensional (perimeter-based) fractal dimension, $D_{pf} \approx 1.15$. From the measured $D_{pf}$, by applying the semiempirical correlations from the literature,[70,71] we have obtained the three-dimensional (mass) fractal dimension, $D_f = 2.7$. This again confirms the $D_f$ value obtained above from the PBE approach.

The absence of a temperature influence on the structure of the TFE20 clusters in the temperature range of 25−70 °C deserves some further discussion. Having observed partial coalescence at 25 °C, one would expect an increase in coalescence extent with temperature. The fact that this is not the case could be explained by considering that TFE is not homogeneously distributed along the polymer chains, since otherwise the polymer viscosity should be sensitive to the temperature increase, leading to changes in the coalescence extent. Instead, polymerized TFE (PTFE) chains might be present as a different phase inside the particle (e.g., in form of rigid TFE-rich domains dispersed in the main elastomer phase). Since PTFE is a crystalline polymer, the TFE-rich (e.g., impure PTFE) domains inside the elastomer particles are the key resistance against coalescence. Since their rigidity is not altered in the given temperature range, it follows that the coalescence extent is independent of temperature.

**4.3. DLCA Kinetics of the High TFE Elastomer Colloids.** As mentioned previously, since the refractive index of the particles in the TFE75-A and -B latices is almost equal to that of water, the scattered light intensity from the particles as well as the clusters is too low to have good statistics for the light scattering measurements. Thus, we have added urea at a concentration of 2.0 mol/L in all the aggregating systems to increase the contrast for the DLS measurements. This also increases the dispersant viscosity by 10%,[66] which has been accounted for in measurement and computation of $\langle R_h \rangle$ as well as in the PBE modeling. Since both TFE75-A and -B latices have a similar CCC of about 0.4 mol/L, the DLCA experiments were carried out at a $HNO_3$ concentration of 1.0 mol/L at all three temperatures (25, 50, and 70 °C). It is found that, similar to the case of the TFE20 latex, the $\langle R_h \rangle$ increment increases as temperature increases for both TFE75-A and -B latices, as shown in Figure 9. When all the $\langle R_h \rangle$ data obtained for both latices at different temperatures are plotted as a function of the dimensionless time $\tau$, however, they all collapse onto a single master-curve, as reported in Figure 10. This means that the clusters formed by both TFE75-A and -B

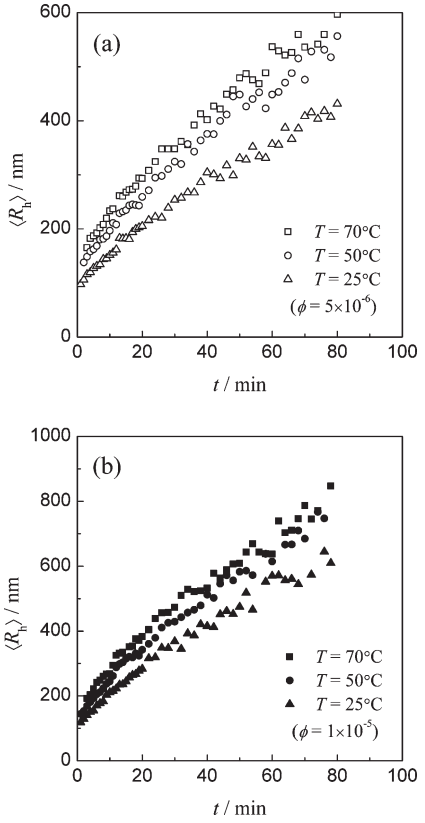


**Figure 9.** Time evolutions of $\langle R_h \rangle$ for (a) the TFE75-A latex at $\phi = 5.0 \times 10^{-6}$ and (b) the TFE75-B latex at $\phi = 1.0 \times 10^{-5}$ in DLCA, destabilized by $HNO_3$ at three different temperatures.

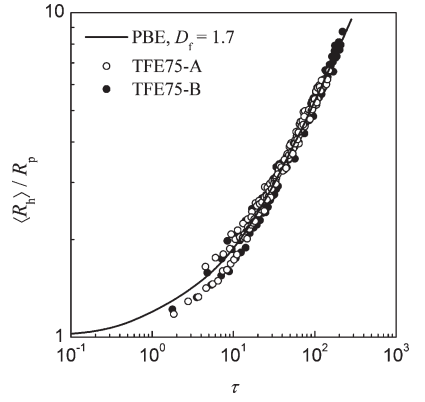


**Figure 10.** $\langle R_h \rangle$ data, measured for the TFE75-A latex and for the TFE75-B latex at different conditions, plotted versus the dimensionless time $\tau$. The solid curve is the PBE simulation with $D_f = 1.7$.

latices at different temperatures have the same structure. For sufficiently large $\tau$, the measured size evolutions will eventually obey the power-law scaling with a slope of $0.59 = 1/D_f$, and it follows that $D_f = 1.7$, a typical $D_f$ value for ramified fractal clusters under DLCA conditions.[10−26] This means that coalescence is negligible for both TFE75-A and -B latices at different temperatures. In Figure 10, the solid curve is the PBE simulation using $D_f = 1.7$. The good agreement between the experimental data and model predictions confirms the obtained $D_f$ value.

At this point, it becomes crucial to verify the expected tenuous, ramified structure of the clusters by the cyro-SEM technique. By freezing a sample from the aggregation experiment at 25 °C, we have obtained very clear pictures of the fractal clusters, of which an example is shown in Figure 11.

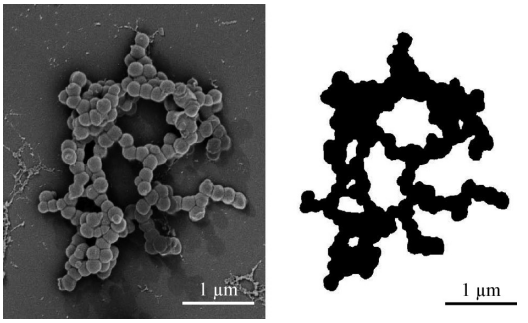


**Figure 11.** Cryo-SEM image of a typical TFE75 cluster, grown at 25 °C. From the projection area (picture on the right side) the fractal dimension of the object is estimated by the box counting method.

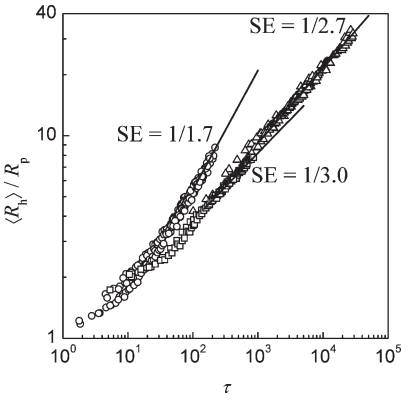


**Figure 12.** Summary of the $\langle R_h \rangle$ data under DLCA for all the latices examined in this work as a function of the dimensionless time $\tau$, where the scaling exponent gives $SE = 1/D_f$ (straight lines). The symbols correspond to the TFE0-A and -B latices at 25 °C (□), TFE20 latex at 25, 50, and 70 °C (△), and TFE75-A and B latices at 25, 50, and 70 °C (○).

Actually, the distinct boundaries among the particles in the cluster demonstrate the absence of coalescence among the particles, although some deformation is apparent. Evaluation of the projection area of the binary images, as shown in Figure 11, for 15 clusters of micrometer size by box counting[8,72−74] yields $D_f = 1.7 \pm 0.1$, which is again in good agreement with the value from the PBE simulations.

It should be noted that it is not surprising for the particles of the TFE75-A and -B latices containing a dominant fraction of TFE (75%) to behave like rigid particles under DLCA conditions if we recall the argument put forward above for the TFE20 latex. Let us consider again that the 75% TFE are dispersed in the form of small domains within the primary particles. Then, the volume fraction of TFE-rich domains is well around the densest packing limit.[76] This would mean that the PTFE-like phase inside the primary particles is jammed and the elastomer phase is located in the void of the jammed phase. Therefore, under such conditions, coalescence between particles could hardly occur.

To have a general view of the effect of the cluster structure (due to the coalescence extent) on the aggregation kinetics, we have summarized the $\langle R_h \rangle$ evolutions as a function of the dimensionless time $\tau$ from all the three classes of particles in Figure 12. As can be seen, the shape of the master-curve is very sensitive to the fractal dimension (inverse of the scaling exponent, SE). Since in the diffusion limit the fractal dimension is the only parameter in the PBE model, through the DLCA experiments and then the PBE simulations, one can reliably estimate the value of the fractal dimension, which quantifies the coalescence extent of soft particles, as is the case for our rubber colloid.

## 5. Conclusions

In this work, we have studied the effect of polymer composition on the coalescence behavior of elastomer particles during fast, diffusion-limited aggregation, for five different latices with a similar glass transition temperature (about −20 °C) but with different polymer viscosities (i.e., molecular weights) and tetrafluoroethylene (TFE) fractions within the primary particles. The methodology used to quantify the coalescence extent is to determine the fractal dimension (structure) of the clusters formed during aggregation. In particular, we first measure in situ the time evolution of the average hydrodynamic radius of the clusters using dynamic light scattering for each latex at different aggregation temperatures (25−70 °C). Then, we apply the Smoluchowski kinetic approach, based on population balance equations (PBE), to simulate the measured kinetics using the fractal dimension $D_f$, the only unknown parameter, as the fit parameter.

It is found that the obtained $D_f$ value from the PBE simulations is well correlated to the TFE content within the primary particles, with a $D_f$ value equal to 3 in the absence of TFE, 2.7 with 20% TFE, and 1.7 with 75% TFE. These results indicate that in the absence of TFE clusters coalesce completely during aggregation, with $D_f = 3.0$. Then, as the TFE fraction within the primary particles increases, the coalescence extent decreases progressively. At 75% TFE content, the particles do not coalesce, forming basically fractal clusters as if they were rigid particles. To confirm the structure information obtained from the PBE simulations, we have also made images of the clusters using the cryogenic scanning electron microscopy technique. Both the shape of the clusters and the $D_f$ values obtained from the image analysis are in good agreement with the PBE results. It is therefore concluded that measuring the fast, diffusion-limited aggregation kinetics combined with the PBE simulations is a reliable methodology to investigate the coalescence behavior of elastomer colloids for example.

The insensitivity of the coalescence extent to the aggregation temperature in the range between 25 and 70 °C supports that the presence of TFE is the key factor controlling coalescence. Furthermore, it reveals that the polymerized TFE (PTFE) is probably not homogeneously distributed among the polymer chains, and it might be present in very small, segregated TFE-rich domains within the primary particles. In this way, since the PTFE-like phase is rigid in the given temperature range, it follows that the coalescence extent does not change with temperature. It should be noted, however, that the control of elastomer particle coalescence by the polymer composition can be complementary to the effect of fixed surface charges, which has been explored in a parallel study[77] by temperature-dependent cluster coalescence of a TFE free elastomer colloid. Thus, manipulation of the bulk polymer phase as well as particle surface properties provides tools to design rubbery materials with an adjustable degree of coalescence for various applications.

**Acknowledgment.** The Electron Microscopy Center of ETH Zurich (EMEZ), especially Roger Wepf, is appreciated for the support in cryo-SEM as well as Frank Krumeich for his support in conventional SEM. We thank Kirill Feldman from the Institute of Polymers (ETH Zurich) for running DSC. This work has largely benefited from discussions with Miroslav Soos. Latex supply by Solvay Solexis and funding by the Swiss National Science Foundation (Grant 200020-113805/1) are gratefully acknowledged.

**Supporting Information Available:** SI-Figure 1 reports results of differential scanning calorimetry (DSC) tests for the elastomers containing 0, 20, and 75% TFE in the polymer phase, which are compared to pure PTFE; the results support our proposed explanation that polymer rigidity, and therefore the extent of cluster coalescence, is related to the existence of TFE-rich domains. This material is available free of charge via the Internet at http://pubs.acs.org.

## References and Notes

(1) Mazur, S. Coalescence of Polymer Particles. In *Polymer Powder Technology*; Narkis, M., Rosenzweig, N., Eds.; Wiley: Chichester, UK, 1995; Chapter 8, pp 157−216.
(2) Keddie, J. L. *Mater. Sci. Eng., R* **1997**, *21*, 101–170.
(3) Fitch, R. M. *Polymer Colloids*; Academic Press: San Diego, 1997.
(4) *Modern Plastics Handbook*; Harper, C. A., Ed.; McGraw-Hill: New York, 2000.
(5) Ebnesajjad, S. *Fluoroplastics*; Plastics Design Library: Norwich, 2003; Vol. *2*.
(6) Gauer, C.; Jia, Z.; Wu, H.; Morbidelli, M. *Langmuir* **2009**, *25*, 9703–9713.
(7) Gauer, C.; Wu, H.; Morbidelli, M. *Langmuir* **2009**, *25*, 12073–12083.
(8) Jullien, R.; Botet, R. *Aggregation and Fractal Aggregates*; World Scientific: Singapore, 1987.
(9) Meakin, P. *Adv. Colloid Interface Sci.* **1988**, *28*, 249–331.
(10) Lin, M. Y.; Lindsay, H. M.; Weitz, D. A.; Klein, R.; Ball, R. C.; Meakin, P. *J. Phys.: Condens. Matter* **1990**, *2*, 3093–3113.
(11) Weitz, D. A.; Oliveria, M. *Phys. Rev. Lett.* **1984**, *52*, 1433–1436.
(12) Weitz, D. A.; Huang, J. S.; Lin, M. Y.; Sung, J. *Phys. Rev. Lett.* **1984**, *53*, 1657–1660.
(13) Aubert, C.; Cannell, D. S. *Phys. Rev. Lett.* **1986**, *56*, 738–741.
(14) Bolle, G.; Cametti, C.; Codastefano, P.; Tartaglia, P. *Phys. Rev. A* **1987**, *35*, 837–841.
(15) Lin, M. Y.; Lindsay, H. M.; Weitz, D. A.; Ball, R. C.; Klein, R.; Meakin, P. *Nature* **1989**, *339*, 360–362.
(16) Midmore, B. R. *J. Chem. Soc., Faraday Trans.* **1990**, *86*, 3763–3768.
(17) Martin, J. E.; Wilcoxon, J. P.; Schaefer, D.; Odinek, J. *Phys. Rev. A* **1990**, *41*, 4379–4391.
(18) Carpineti, M.; Ferri, F.; Giglio, M.; Paganini, E.; Perini, U. *Phys. Rev. A* **1990**, *42*, 7347–7354.
(19) Shih, W. Y.; Liu, J.; Shih, W.-H.; Aksay, I. A. *J. Stat. Phys.* **1991**, *62*, 961–984.
(20) Zhou, Z.; Chu, B. *J. Colloid Interface Sci.* **1991**, *143*, 356–365.
(21) Burns, J. L.; Yan, Y. D.; Jameson, G. J.; Biggs, S. *Langmuir* **1997**, *13*, 6413–6420.
(22) Tirado-Miranda, M.; Schmitt, A.; Callejas-Fernandez, J.; Fernandez-Barbero, A. *Langmuir* **1999**, *15*, 3437–3444.
(23) Tirado-Miranda, M.; Schmitt, A.; Callejas-Fernandez, J.; Fernandez-Barbero, A. *Phys. Rev. E* **2003**, *67*, 011402.
(24) Wu, H.; Lattuada, M.; Sandkuhler, P.; Sefcik, J.; Morbidelli, M. *Langmuir* **2003**, *19*, 10710–10718.
(25) Sandkuhler, P.; Sefcik, J.; Morbidelli, M. *Adv. Colloid Interface Sci.* **2004**, *108*, 133–143.
(26) Berka, M.; Rice, J. A. *Langmuir* **2005**, *21*, 1223–1229.
(27) Lattuada, M.; Wu, H.; Sandkuhler, P.; Sefcik, J.; Morbidelli, M. *Chem. Eng. Sci.* **2004**, *59*, 1783–1798.
(28) Wu, H.; Xie, J.; Morbidelli, M. *Biomacromolecules* **2005**, *6*, 3189–3197.
(29) von Smoluchowski, M. *Z. Phys. Chem.* (*Munich*) **1917**, *92*, 129–168.
(30) Ziff, R. M.; McGrady, E. D.; Meakin, P. *J. Chem. Phys.* **1985**, *82*, 5269–5274.
(31) Meakin, P.; Chen, Z. Y.; Deutch, J. M. *J. Chem. Phys.* **1985**, *82*, 3786–3789.
(32) Ramkrishna, D. *Population Balances*; Academic Press: San Diego, 2000.
(33) Higashitani, K.; Matsuno, Y. *J. Chem. Eng. Jpn.* **1979**, *12*, 460–465.
(34) Broide, M. L.; Cohen, R. J. *J. Colloid Interface Sci.* **1992**, *153*, 493–508.
(35) Elimelech, M.; Gregory, J.; Jia, X.; Williams, R. A. *Particle Deposition and Aggregation*; Butterworth-Heinemann: Woburn, 1995.
(36) Odriozola, G.; Schmitt, A.; Callejas-Fernandez, J.; Martinez-Garcia, R.; Hidalgo-Alvarez, R. *J. Chem. Phys.* **1999**, *111*, 7657–7667.
(37) Lattuada, M.; Wu, H.; Sefcik, J.; Morbidelli, M. *J. Phys. Chem. B* **2006**, *110*, 6574–6586.
(38) Fuchs, N. *Z. Phys.* **1934**, *89*, 736–743.
(39) Spielman, L. A. *J. Colloid Interface Sci.* **1970**, *33*, 562–571.
(40) Israelachvili, J. N. *Intermolecular and Surface Forces*; Academic Press: London, 1992.

(41) Thompson, D. W.; Collins, I. R. *J. Colloid Interface Sci.* **1994**, *163*, 347–354.
(42) Runkana, V.; Somasundaran, P.; Kapur, P. C. *AIChE J.* **2005**, *51*, 1233–1245.
(43) Jia, Z. C.; Gauer, C.; Wu, H.; Morbidelli, M.; Chittofrati, A.; Apostolo, M. *J. Colloid Interface Sci.* **2006**, *302*, 187–202.
(44) van Zanten, J. H.; Elimelech, M. *J. Colloid Interface Sci.* **1992**, *154*, 1–7.
(45) Ryde, N.; Matijevic, E. *J. Chem. Soc., Faraday Trans.* **1994**, *90*, 167–171.
(46) Hanus, L. H.; Hartzler, R. U.; Wagner, N. J. *Langmuir* **2001**, *17*, 3136–3147.
(47) Herrington, T. M.; Midmore, B. R. *J. Chem. Soc., Faraday Trans. 1* **1989**, *85*, 3529–3536.
(48) Holthoff, H.; Egelhaaf, S. U.; Borkovec, M.; Schurtenberger, P.; Sticher, H. *Langmuir* **1996**, *12*, 5541–5549.
(49) Berka, M.; Rice, J. A. *Langmuir* **2004**, *20*, 6152–6157.
(50) van Dongen, P. G. J.; Ernst, M. H. *Phys. Rev. Lett.* **1985**, *54*, 1396–1399.
(51) Vemury, S.; Pratsinis, S. E. *J. Aerosol Sci.* **1995**, *26*, 175–185.
(52) Sandkuhler, P.; Lattuada, L.; Wu, H.; Sefcik, J.; Morbidelli, M. *Adv. Colloid Interface Sci.* **2005**, *113*, 65–83.
(53) Lattuada, M.; Sandkuhler, P.; Wu, H.; Sefcik, J.; Morbidelli, M. *Adv. Colloid Interface Sci.* **2003**, *103*, 33–56.
(54) Sandkuhler, P.; Sefcik, J.; Morbidelli, M. *J. Phys. Chem. B* **2004**, *108*, 20105–20121.
(55) Jia, Z.; Wu, H.; Xie, J. J.; Morbidelli, M. *Langmuir* **2007**, *23*, 10323–10332.
(56) Finsy, R. *Adv. Colloid Interface Sci.* **1994**, *52*, 79–143.
(57) Kerker, M. *The Scattering of Light*; Academic Press: New York, 1969.
(58) Wiscombe, W. J. Mie Scattering Calculations: Advances in Technique and Fast, Vector-Speed Computer Codes. NCAR Technical Note NCAR/TN-140+STR; National Center for Atmospheric Research: Boulder, CO, **1979** (1996 revised).
(59) Fisher, M. E.; Burford, F. J. *Phys. Rev.* **1967**, *156*, 583–622.
(60) Sorensen, C. M. *Aerosol Sci. Technol.* **2001**, *35*, 648–687.
(61) Lattuada, M.; Wu, H.; Morbidelli, M. *J. Colloid Interface Sci.* **2003**, *268*, 96–105.
(62) Lattuada, M.; Wu, H.; Morbidelli, M. *J. Colloid Interface Sci.* **2003**, *268*, 106–120.
(63) Lattuada, M. PhD Thesis, No. 15187, ETH Zurich, Switzerland, **2003**.
(64) Koppel, D. E. *J. Chem. Phys.* **1972**, *57*, 4814–4820.
(65) *Neutrons, X-rays and Light: Scattering Methods Applied to Soft Condensed Matter*; Lindner, P., Zemb, T., Eds.; Elsevier: Amsterdam, 2002.
(66) *CRC Handbook of Chemistry and Physics*, 88th ed. (Internet Version 2008); Lide, D. R., Ed.; CRC Press: Boca Raton, FL, 2008; Chapter 8, pp 52−77 (Table: Concentrative Properties of Aqueous Solutions).
(67) Echlin, P. *Low-Temperature Microscopy and Analysis*; Plenum Press: New York, 1992.
(68) Ritter, M.; Henry, D.; Wiesner, S.; Pfeiffer, S.; Wepf, R. A Versatile High-Vacuum Cryo-Transfer for Cryo-FESEM, Cryo-SPM and Other Imaging Techniques. *Microscopy and Microanalysis*; New York, 1999; Suppl. 2, Vol. *5*, pp 424−425.
(69) Mandelbrot, B. B. *The Fractal Geometry of Nature*; Freeman: New York, 1982.
(70) Lee, C.; Kramer, T. A. *Adv. Colloid Interface Sci.* **2004**, *112*, 49–57.
(71) Ehrl, L.; Soos, M.; Lattuada, M. *J. Phys. Chem. B* **2009**, *113*, 10587–10599.
(72) Bushell, G. C.; Yan, Y. D.; Woodfield, D.; Raper, J.; Amal, R. *Adv. Colloid Interface Sci.* **2002**, *95*, 1–50.
(73) Forrest, S. R.; Witten, T. A. *J. Phys. A: Math. Gen.* **1979**, *12*, L109–L117.
(74) *The Fractal Approach to Heterogeneous Chemistry*; Avnir, D., Ed.; Wiley: Chichester, UK, 1989.
(75) Smith, T. G.; Lange, G. D.; Marks, W. B. *J. Neurosci. Methods* **1996**, *69*, 123–136.
(76) Torquato, S.; Truskett, T. M.; Debenedetti, P. G. *Phys. Rev. Lett.* **2000**, *84*, 2064–2067.
(77) Gauer, C.; Wu, H.; Morbidelli, M. *J. Phys. Chem. B*, submitted 2009.